Numerical study of advanced friction modelling for sheet metal forming: Influence of the die local roughness

Alaitz Zabala [a], Eneko Sáenz de Argandoña [a], Daniel Cañizares [b], Iñigo Llavori [a], Nagore Otegi [a], Joseba Mendiguren [a,*]

[a] *Mondragon Unibertsitatea, Faculty of Engineering, Mechanics and Industrial Production, Loramendi 4, Mondragon 20500, Gipuzkoa, Spain*
[b] *Autoform Engineering S L, Carrer de Joan d'Àustria, 116, 08018 Barcelona, Spain*

A R T I C L E   I N F O

A B S T R A C T

Numerical simulation of sheet metal forming processes has become indispensable in the last decades. Although the complexity of the frictional behaviour is identified as a key factor for the prediction accuracy, the industry commonly considers a constant friction coefficient for the whole tool. Furthermore, the influence of roughness distribution of the tool in the friction behaviour has not yet been addressed. In this study the influence of the die local roughness in an advanced friction model has been evaluated in three industrial automotive components. The newly implemented advanced friction model (TriboZone) is suggested for advance or mature process verifications.

1. Introduction

Sheet metal forming stamping is one of the most frequently used manufacturing technologies for mass production. Due to its short lead time and optimum cost efficiency, it is one of the primary technologies in the automotive and packaging industries, being these ones the reference of mass production markets. Stamping requires two items of hardware, namely the press and the tooling/die set. The press is the main hardware and created the force needed to form the sheet material into the desired shape. It can be used for different product manufacturing. The tooling/die set, however, is specific to the component. It is designed to transform the flat blank into the final shape tamping (driven by the press). For a more detailed description, the reader is referred to Böhm and Meurer's work regarding machining trajectory definitions [1].

The die set is usually composed of a punch, a die, and a blank-holder or binder (as shown by Sigvant et al. for the rear door inner of the Volvo XC90 [2]). Each tool can be manufactured out of a net-shape casted material (as shown by Pilthammar et al. for the same Volvo component [3]), or from a laminated bulk tool steel (as used by Pereira et al. in their wear study [4]). In both cases, the toolmakers have to mill the starting material into the desired shape before polishing the tool surfaces until the necessary functional roughness is achieved. Once the tool shape has been carved and the desired surface roughness obtained, the tool set proceeds to a try-out step in which, with the help of blue ink, the

spotting of the die is performed. The shape of the tool is then often slightly modified in order to meet the client's requirements. The complexity of this spotting process can be shown in the work of Zabala et al. regarding the decryption of the blue ink pattern [5] and the work of Essig et al. on the optical metrology of the pattern itself [6]. It accounts for about 24% of the workload of constructing a die set.

The use of numerical simulation has become critical in recent decades as a means of optimising tool shape by predicting the outcome of the forming process. This allows significant reductions in the try-out time and effort [7]. Numerous examples can be found in the literature in which the accuracy of the simulations is studied; these include analysis of the impact of material modelling, boundary conditions and tribological aspects. Of these, material modelling has been the most thoroughly investigated and has been the subject of a significant number of published works over the last 50 years. Examples include the advance model of Barlat et al. for distortional behaviours [8], the advance inelastic models of Sun et al. using the quasi-elastic-plastic hypothesis [9], or the work of Mendiguren et al. on the use of fractional derivatives [10]. Unlike material model input, boundary conditions such as press behaviour and press speed have been not studied in great depth. Pilthammar et al. analysed the impact of the press/die deflection on the process [11] and highlighted the critical effect of the deflection, while Sigvant et al. analysed the impact of the press speed (derived into strain rate) over an industrial component [2]. Both studies highlighted the low

---

Table 1
Industrial benchmark tool roughness summary.

Industrial Benchmark	Tool roughness	References
Volvo XC90 door inner	Ra of 0.35 μm	[2]
Numisheet fender	Sa between 0.2 μm (fine polish) and 0.4 μm (normal polish)	[24]
Opel Insignia B spare wheel	Sa roughness ranged from 0.65 μm to 2.32 μm with an average of 1.12 μm	[18]
Rear door inner for Volvo XC90	Sa between 0.35 μm and 0.75 μm for the laser hardened binder and Sa between 0.2 μm and 0.5 μm for the chrome-plated die and punch	[23]
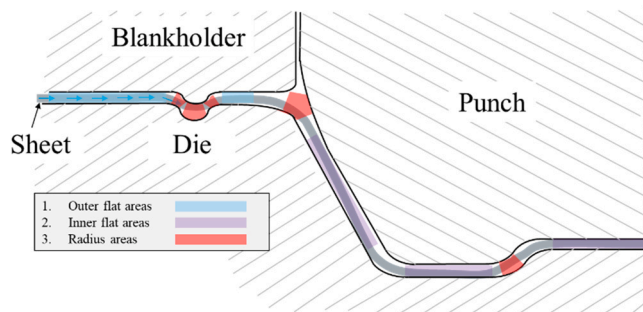
Fig. 1. Definition of the different effective areas of the tooling.

level of information and research on these topics and concluded that this could have a critical impact on the outcome of the prediction.

Research on the tribological behaviour (e.g. friction, wear and galling) of sheet metal forming has gained increasing relevance in recent years. Numerous studies have been carried out regarding these topics. It has been proven that the friction coefficient of a tribological system is highly dependent on the contact pressure (as shown by Szakaly and Lenard in their analysis of the influence parameters on flat-die friction behaviour [12]). This effect is related to the asperity flattening due to the friction (as investigated by Shisode et al. in their work on tribological modelling [13]). Several studies have been performed on this topic with the aim of correctly modelling the effect of the asperity deformation/wearing-off to correctly predict the friction coefficient during the process. An example of this is found in Mishra et al.'s analysis of single-asperity sliding contact modelling [14]. Equally, the impact of the sheet material surface strain and sliding velocity has been shown to have a strong effect on the friction coefficient of the tribological pair.The aforementioned work of Sigvant et al. on strain rate [2], the work of Masters et al. on strip draw test results of pre-stretched high strength automotive aluminium alloys [15] and the analysis of the real area of contact due to the normal load and sub-surface straining work presented by Shisode et al. [16] can be mentioned as examples. Additionally, the temperature increase that occurs in dies during the continuous process has been a topic of interest in the recent years. Several studies agree on the relevant impact of the variation in friction when increasing the temperature. Heingärtner et al. analysed the process control to compensate for the temperature-induced friction changes [17], while the work of Kott et al. focused on the control of the Opel Insignia B component critical to the temperature changes [18]. Waanders et al. worked on phenomenological modelling [19] and Veldhuis et al. focused on the physical based friction modelling of cup drawing simulations [20]. Hettich et al. worked on lubricant and scrap reduction to understand the evolution of friction behaviour with the increase of temperature during the process [21].

The aforementioned studies show the complexity of the frictional behaviour of a tribological system and highlight how this can affect the outcome of a forming simulation. In terms of friction modelling, one of

the main breakthrough steps in the last decade has been provided by Hol and Wiebenga with the development of the TriboForm® software. This software can model the behaviour of the friction coefficient under strain, temperature, sliding velocity and pressure conditions and analyse the impact of the variables on industrial automotive components. The impact has been analysed for a door outer of the Mercedes Benz C-class Coupé [22], a rear door inner of the Volvo XC90 [23] (including die deflection combination [3] and robustness analysis [7]), a fender part of Numisheet 2002 benchmark [24], a Volvo V60 fender, front door inner and front door ring-frame [25] and an ASPECT project Philips consumer good component [19]. These benchmark cases have helped increase interest in the topic by highlighting the impact that tribology has on real-world industry cases.

One of the key input data for the tribological model is the die surface topography. Table 1 shows the industrial tool surface roughness data reported in the above-mentioned studies, which ranges from Sa/Ra 0.2–2.32 μm.

It should be highlighted that the effect of using different tool roughness in the simulation accuracy was studied in the above-mentioned study by Sigvant et al. They concluded that it had a significant effect on the predicted stretching and flow of the material.

The reviewed studies suggest that accurate characterisation of tool roughness is key for the correct modelling of friction behaviour. However, even if the presence of heterogeneous roughness along the tool is known (i.e., the 0.65–2.32 μm range of the Opel Insignia B spare wheel), the impact of considering that roughness heterogeneity on the forming simulation has yet not been studied. Therefore, the main objective of this study was to evaluate the potential impact of the local tool roughness consideration in an industrial automotive deep drawing numerical simulation. First, a large-scale roughness measurement campaign was conducted across different automotive industrial tooling. Second, three representative automotive components were selected in which the tribological behaviour had a critical impact (two fenders and an inner door panel). Third, different tribological models were constructed by increasing the complexity. These ranged from the classic constant Amonton-Coulomb model to a consideration of the local roughness. The three components were simulated under the different tribological models and the impact of each assumption was evaluated. The aim was to establish whether considering the influence of local die roughness would be worthwhile in future investigations.

2. Experimental analysis

This section presents the large-scale roughness measurement campaign conducted in different automotive industrial tooling sets.

2.1. Industrial tooling roughness measurement procedure

In order to obtain a representative amount of data, roughness measurements were conducted across more than 25 different industrial tools. The measurement campaign was conducted in an automotive tool-maker workshop and all surfaces were prepared to the required quality (fineness) under industrial standards.

Every tool was divided in three different effective areas depending on their geometry, features and localisation (a detail of the areas can be found in Fig. 1):

1. *Outer flat areas.* These areas correspond to the flat areas of the tooling located on the blank-holder tool or on the die tool out of the drawing cavity. These areas represent the flat areas in which the restraining of the draw-in is performed by the compression between the blank-holder and the die.
2. *Inner flat areas.* The inner flat areas are defined as the flat areas within the drawing cavity on both die and punch tools.
3. *Radius areas.* These encompass all radius areas from the inner (drawing cavity) and the outer side as well as the draw-bead features.
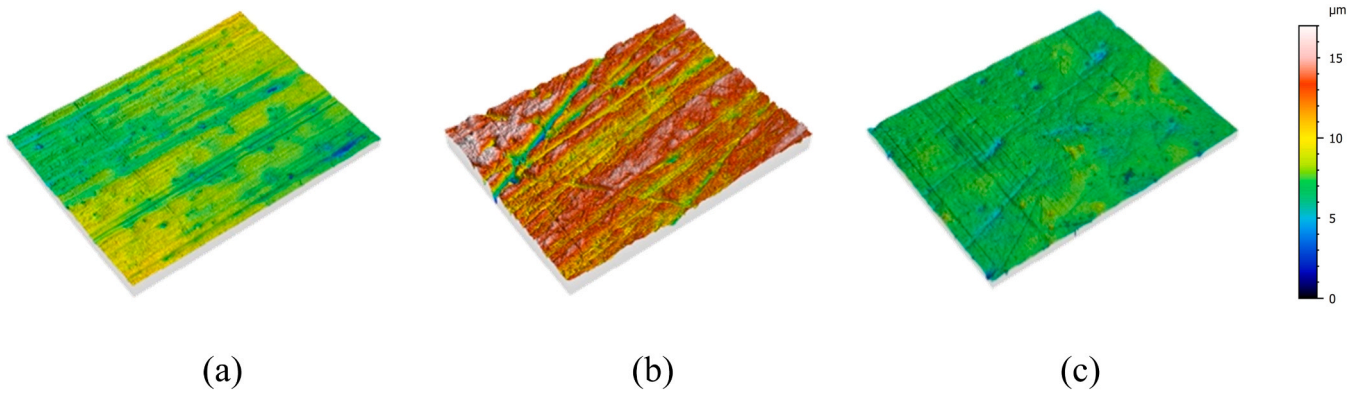
Fig. 2. Representative axonometric projections of the measurements corresponding to the three effective areas of the tooling (depicted at the same scale for comparison purposes): (a) Outer flat area, (b) inner flat area, and (c) radius area.

At least three measurements were taken from each effective area at each set of tools, resulting in a global amount of > 190 measurements evaluated.

It is known from both the existing literature [4] and industry experience that each sheet material family (i.e., coated steels, uncoated steels, aluminium) requires different roughness finesses in order to assure the tool quality under a large volume of forming operations. With the aim of having a representative overview of the industrial quality, the analysed automotive tooling covered a large range of component materials. In the case of steel components, this covered mild steel components to high strength steel reinforcements; in the case of aluminium components, this covered AA6xxx family exterior panels to AA5xxx interior reinforcements. All were industrial tool sets and therefore the roughness quality met the required industrial standards. No coated tools were studied in this work.

A surface replication technique was used for high-resolution surface roughness characterisation. First, the surface was cleaned with acetone using lint-free wipes to eliminate any residue. A high-resolution light-curing resin (Technovit) was then applied on the desired surface using a syringe. Next, the resin was light-cured for 20–60 s using a light-curing lamp (Technovit Blue lamp). The replicas were then analysed in the laboratory with a SensoFar S-NEOX optical profilometer using inter-ferometry technique (20x DI objective, acquisition area: $877 \times 660 \ \mu m^2$). SensoMap Premium 7.4 metrology software was used for data post-processing, computing surface topography parameters on the primary S-F surface in accordance with ISO 25178 [26]. Due to the extended use of two-dimensional roughness parameters in the industry, die surfaces were also measured using the Mitutoyo SJ10 Surftest pro-filometer (computing the two-dimensional Ra and Rz parameters under ISO 4287:1997 standard for comparison).

From the analysed > 190 representative surface areas, the characteristic features of the surfaces were evaluated using a set of topo-graphical parameters from ISO 25178. These described height (Sa, Sq, Sz, Ssk), spatial (Str, Std), hybrid (Sdq, Sdr) and functional (Vmp, Vvv) properties.

- *S*a: Average roughness. This parameter describes the arithmetic mean of the absolute value of the height within the surface. Together with its analogous two-dimensional Ra parameter, it is the most commonly used surface roughness parameters in industry. However, this height descriptor parameter is insensitive in differentiating peaks, valleys and the spacing of the various surface features (as discussed previously [27]).
- Sz: Maximum height. This parameter describes the extreme characteristic of the surface height as the sum of the maximum value of the surface peak height and the maximum value of the surface valley in a sampling area. Similar to average roughness, Sz/Rz are the most frequently used parameters for controlling the maximum local disruptions of the roughness pattern. This maximum surface peak height is usually the main indicator used to evaluate whether the roughness could lead to the initiation of galling issues during the repetitive use of the tool in mass production volume stamping.
- Sq: Root mean square roughness. This parameter describes the root mean square value of the surface departures within the sampling area, which corresponds to the standard deviation of height distribution. Similar to the previously described Sa, it lacks information about roughness distribution. However, it is more sensitive to vertical outliers than Sa.
- Ssk: Skewness. This parameter is derived from the height distribution curve of the surface and represents the third statistical moment (qualifying the symmetry of the height distribution). It can be used to describe the shape of the height distribution. For a Gaussian surface (which has a symmetrical shape for the surface height distribution), the skewness is zero. A negative Ssk indicates a predominance of valleys, whereas a positive Ssk indicates a predominance of peaks. This presents a strong influence on the tribological behaviour of the contact surfaces, being the negatively skewed surfaces associated to a better tribological performance [28].
- Str: This parameter describes the texture aspect ratio of the surface. It is used to evaluate the surface texture isotropy. It is computed from the auto correlation function [29] and its unitless values lies between 0 and 1. A value near 1 indicates that the surface is isotropic (i.e., it has the same characteristics in all directions). If the value is near 0, the surface is anisotropic (i.e., it has an oriented and/or periodic structure).
- Std: This parameter describes the texture direction of the surface. This parameter is only meaningful for anisotropic surfaces (Str<0.5) since it provides the lay direction of the surface texture. It enables analysis of the orientation of the surface roughness in relation to the material flow direction.
- Sdq: This parameter describes the root mean square surface slope. This is calculated as a root mean square of slopes at all points in the surface (representing the surface micrometry inclination). This is a relevant parameter in tribology since it is related to the ability to the plastic deformation of asperities and to tribological performance [27].
- Sdr: This parameter described the developed interfacial area of a surface. Reported as a percentage value, it is used as a measure of the surface complexity. It represents the percentage of additional surface area contributed by the texture as compared to an ideal plane (i.e., for an ideal flat surface, Sdr = 0).
- Vmp: This parameter describes the peak material volume. It is calculated from the Abbot-Firestone curve (also known as the areal material ratio curve) obtained by the integration of height distribution on the whole surface. This parameter is defined as the material volume- enclosed in the 10% material ratio and normalised to unit
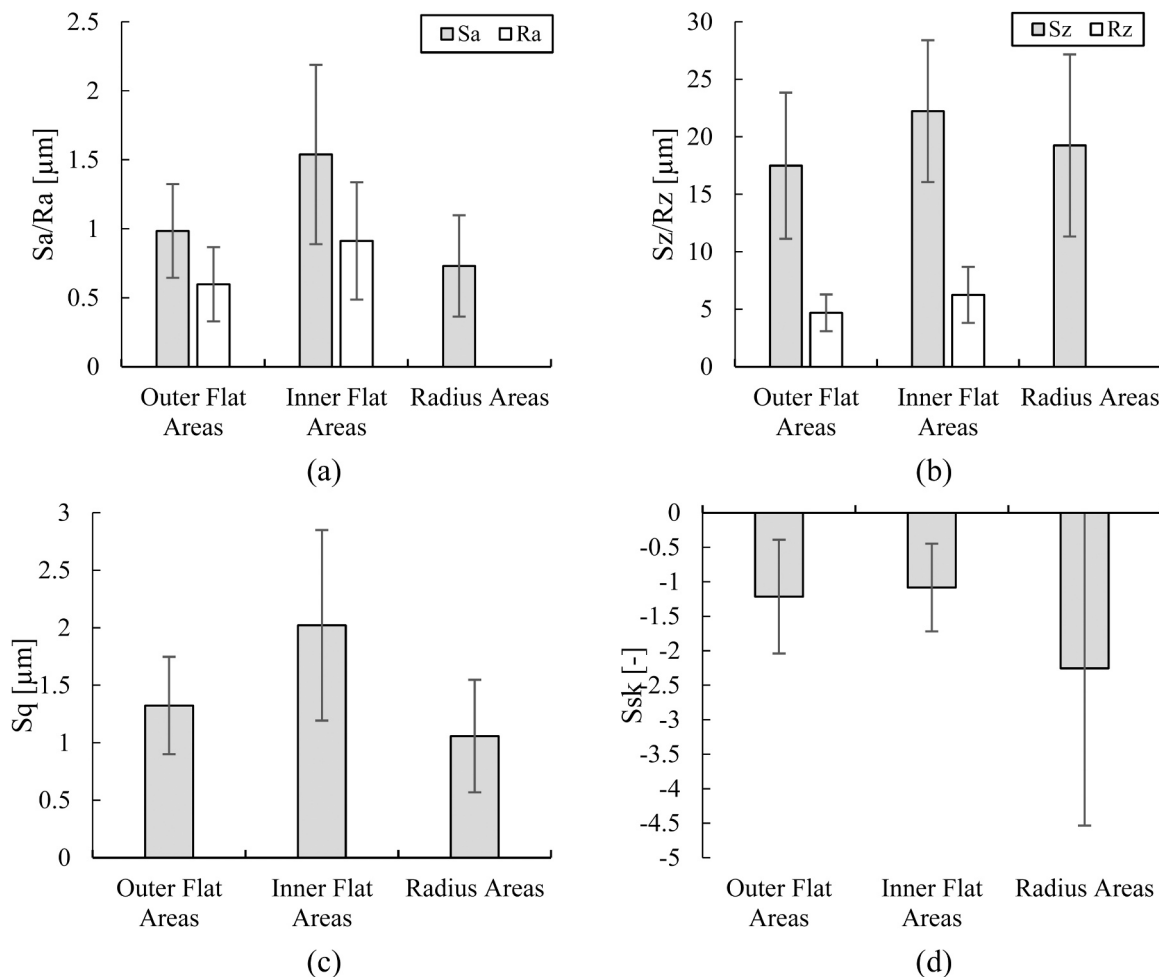
Fig. 3. Height descriptor parameters of the three effective areas (outer flat area, inner flat areas, and radius areas): a) average roughness (Sa/Rz), b) maximum height (Sz/Rz), c) root mean square roughness (Sq), and d) skewness (Ssk).
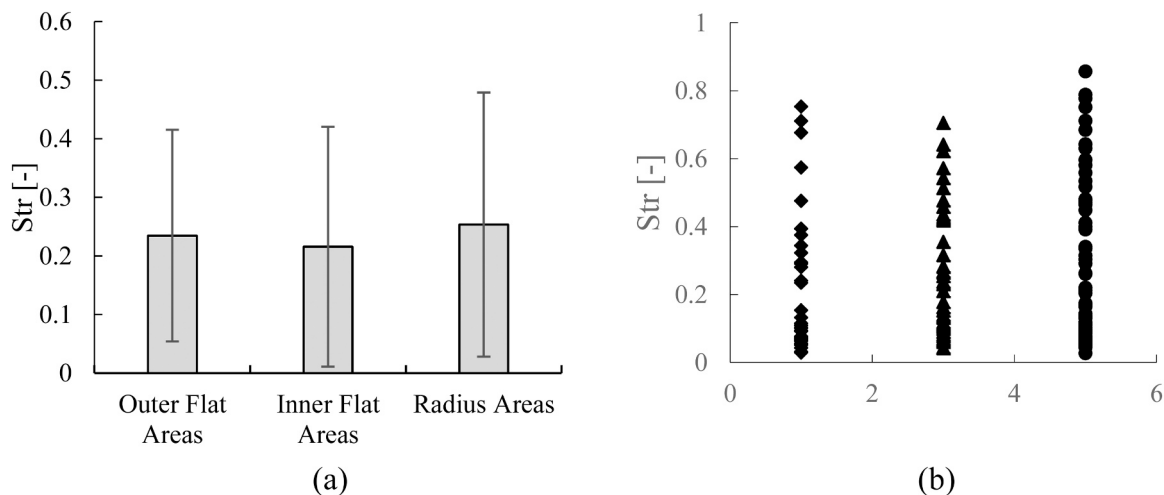

Fig. 4. Lateral descriptor parameter (Str): a) mean value and standard deviation, b) all values.

sampling area. The Vmp parameter characterises the volume of material located on the highest peaks of the surface which are likely to be removed during a wear process.

- Vvv: This parameter describes the void volume. Similar to the previously introduced Vmp, Vvv is calculated from the Abbott firestone curve [29] and represents the void volume in the valley zone from 80% to 100% of the surface material ratio. The Vvv valley void volume represents the volume capable of retaining lubricant and trapping wear or dirt debris.
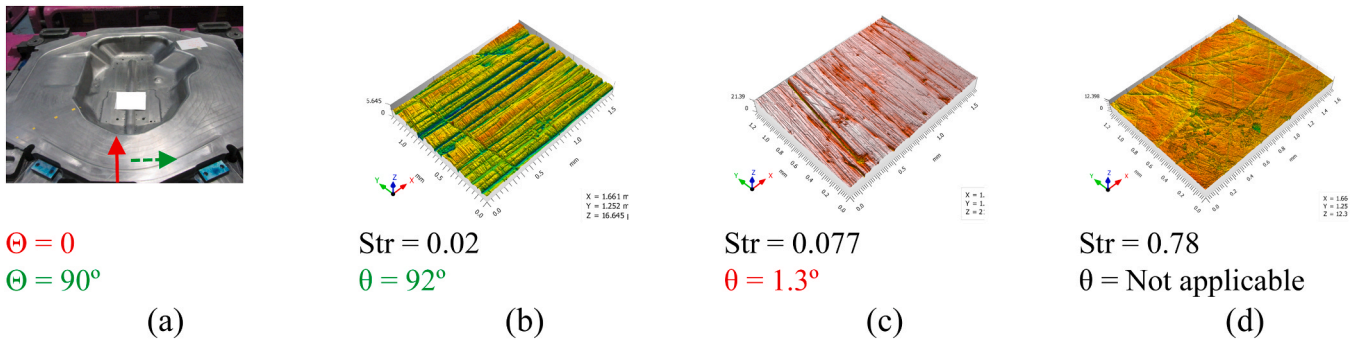
Θ = 0
Θ = 90º
(a)

Str = 0.02
θ = 92º
(b)

Str = 0.077
θ = 1.3º
(c)

Str = 0.78
θ = Not applicable
(d)

Fig. 5. Examples of the surface texture direction parameters: a) image of a die describing the material flow parallel direction (θ = 0º) and the material flow perpendicular direction (θ = 90º); b) representative measurement showing a texture direction perpendicular to the material flow direction; c) representative measurement showing a texture direction parallel to the material flow; and d) representative measurement showing an isotropic surface (no dominant texture direction).
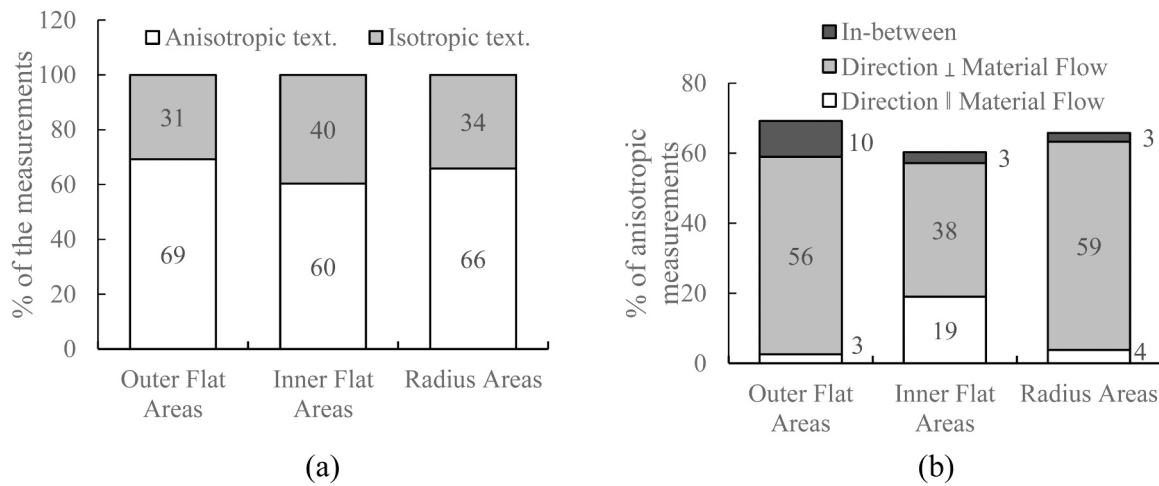

(a)

(b)

Fig. 6. Summary of the surface texture direction study for each effective area: a) percentages of the oriented (anisotropic) and non-oriented (isotropic) texture measurements; b) direction type of the oriented measurements (parallel [∥], perpendicular [⊥], or in-between direction of the texture related to the material flow).
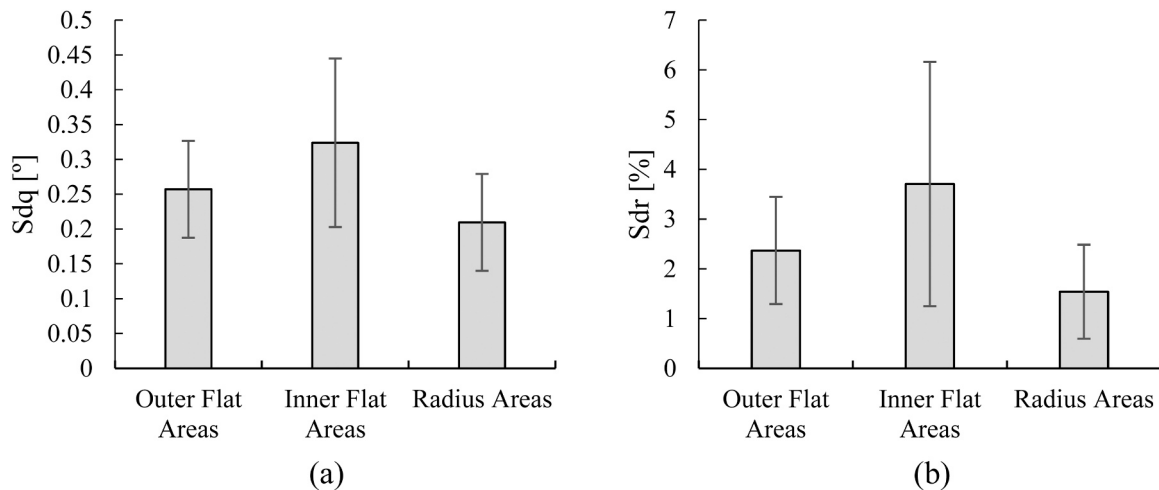

(a)

(b)

Fig. 7. Hybrid topographical parameters: a) root mean square slope of the surface (Sdq); b) developed interfacial area of a surface (Sdr).

2.2. Industrial tooling roughness measurement results and discussion

Fig. 2 presents representative images of the three effective areas. These are depicted at the same scale for comparative purposes. Significant differences can be observed among the different die areas, which means that different polishing degrees were applied along the dies.

Fig. 3 depicts the height descriptor parameters corresponding to the three effective areas of the die.

The average roughness values (Fig. 3 [a]) show that the radius areas presented the lowest average roughness values (Sa). These were
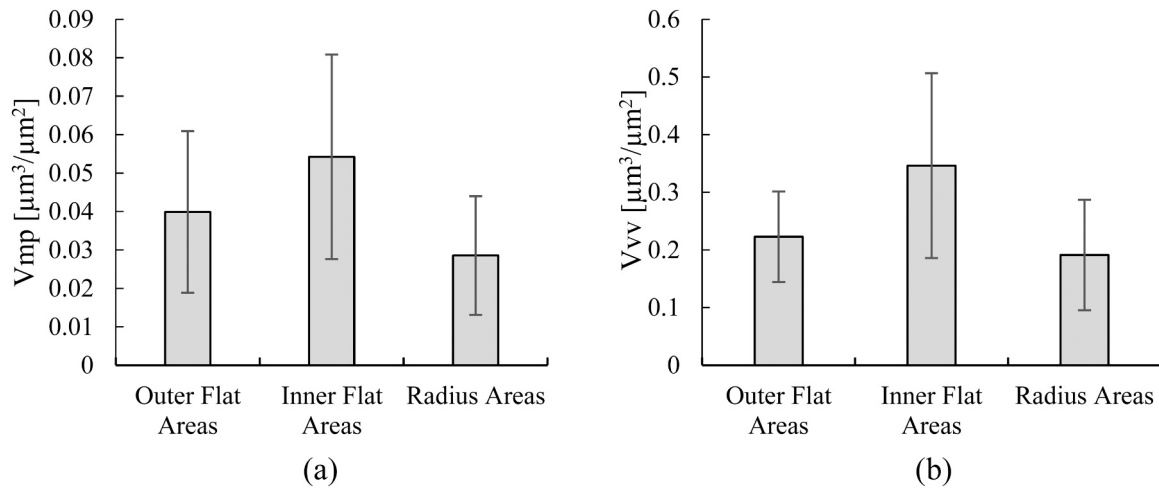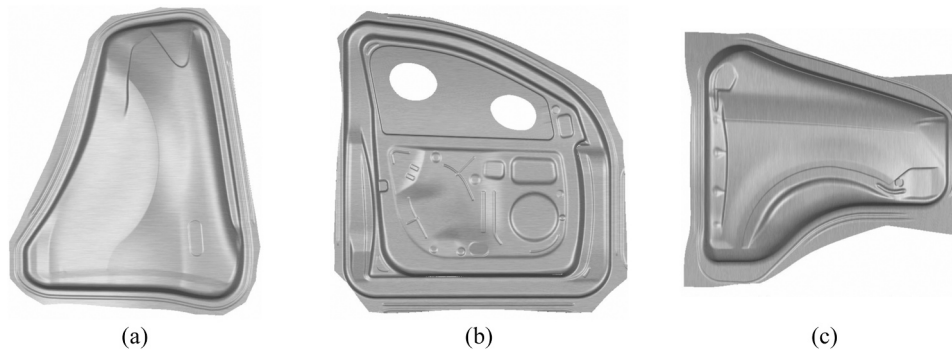
Fig. 8. Peak material and void volume parameters.

Fig. 9. Selected industry benchmark: a) aluminium fender, b) steel door inner and c) steel fender.

Table 2
Main material elasto-plastic properties of the three benchmark cases.

Component	Aluminium fender	Steel door inner	Steel fender
Material	AW-6016-T4	DX56D+Z	Mild steel
Thickness	1.15 mm	1 mm	0.7 mm
Young modulus	70 GPa	210 GPa	210 GPa
Poisson	0.3	0.3	0.3
Hardening model	Swift/Hockett-Sherby	Swift/Hockett-Sherby	Swift/Hockett-Sherby
ε_o	0.00702	0.00869	0.0125
m	0.282	0.266	0.26
C	446.7 MPa	551.4 MPa	656.8 MPa
σ_i	117.3 MPa	160.4 MPa	209.8 MPa
σ_{sat}	309.1 MPa	417.9 MPa	494.2 MPa
a	8.16	5.69	6.18
ρ	0.902	0.827	0.854
α	0.75	0.25	0.25
Yielding model	Barlat-89	Hill	BBC
r_0	0.72	2.05	2.166
r_{45}	0.39	1.73	1.86
r_{90}	0.72	2.5	2.61
σ_0/σ_0	1	1	1
σ_{45}/σ_0	1.0748	1.108	1.0491
σ_{90}/σ_0	1	1.0309	1.0443
r_b	1	0.82	0.83
σ_b/σ_0	0.9813	1.2945	1.3154
M	8	2	6

Table 3
Features of each friction model.

Hypothesis/Friction models	Constant	P-dependent	TriboForm	TriboZone
Sheet material dependency	✔	✔	✔	✔
Pressure dependency		✔	✔	✔
Velocity dependency		✔	✔	✔
Strain dependency			✔	✔
Tool roughness			✔	✔
Local tool roughness distribution				✔

* The P-dependent model could include velocity dependency with a phenomenological approach (not included in the current study).

followed by the outer flat areas, with the inner flat areas being the roughest. The trends were maintained when comparing the 3D Sa with its analogous 2D Ra. However, the 2D parameter presented lower values due to the mechanical filter effect generated by the contact stylus instrument [27]. It should be noted that the radius areas could not be measured with the contact profilometer due to its shape.

As far as the extreme Sz/Rz values were concerned (Fig. 3 [b]), similar values were obtained in the three effective areas. Therefore, it can be concluded that the maximum height was defined by the surface defects and not by the polish degree. Similarly, as with the Sa/Ra values,
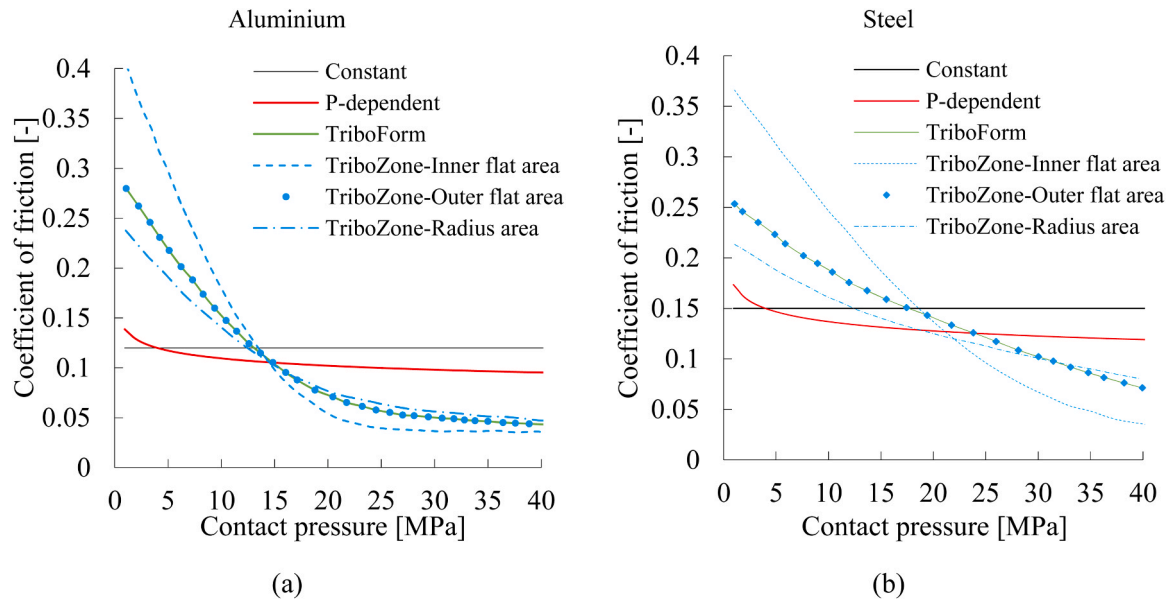
Fig. 10. Dependency of the friction coefficient on the contact pressure for specific conditions (ε ⁻^"p" =0, sliding velocity of 50 mm/s, room temperature) for both tribological cases: a) aluminium alloy sheet material, and b) steel sheet material. a was used on the aluminium fender benchmark and b was used on the steel fender and door inner.

the bidimensional Rz values were significantly lower compared to the three-dimensional Sz values. The root mean square roughness (Sq; Fig. 3 [c]) presented the same trend as observed for the average roughness Sa value. Finally, it can be observed from the skewness value (Ssk; Fig. 3 [d]) that all the effective areas presented negative skews; this indicated a predominance of valleys. Although the radius areas presented a more pronounced preference for valleys, the standard deviation was also bigger. This indicated a bigger scatter among all the measured areas.

The results for the lateral feature descriptor parameter (Str) are depicted in Fig. 4. It can be observed that all the effective zones presented areas with oriented roughness (Str~0) and non-oriented roughness (Str~1) (Fig. 4(a)). A predominance of oriented textures can be observed by looking at the mean values (~0.2). The orientation predominance may have arisen from the milling process traces that were still present on the surface after polishing, the preferred polishing orientation, or a combination of both.

For those surfaces that present anisotropic oriented textures (Str <0.4), the Std parameter represents the texture direction. This is given in degrees between 0° and 180° calculated from a reference (in this case, the horizontal axis referred to 0°). In order to account for the texture direction in terms of the orientation in respect to the material flow, the Std was converted to θ (see Eq. (1)) which provides values from 0° (texture direction parallel to material flow) to 90° (texture direction perpendicular to the material flow). This is shown in Fig. 5.

$$\theta = \text{abs} \quad (Std - 90) \tag{1}$$

Fig. 6(a) summarises the percentages of the oriented (anisotropic) and non-oriented (isotropic) surface textures encountered in the three effective areas. It can be observed that around 65% of the measurements corresponded to anisotropic oriented textures for all effective areas. As far as the orientation direction is concerned, all of the effective areas preferentially presented roughness directions perpendicular to the material flow (θ > 70°), albeit to a different extent. The inner flat areas presented the maximum amount of material flow-oriented surface textures (θ < 30°). All of the effective areas presented some textures that ranged between these two values (30°<θ < 70°), termed as "in between".

Hybrid parameters are shown in Fig. 7. The trends encountered for both the root mean square slope of the surface (Sdq) and the developed

interfacial area of a surface (Sdr) corresponded to those shown by the average roughness (Sa) parameter. The rougher zone (inner flat area) is the one showing the more complex surface (Sdr) and the biggest mean slopes (Sdq), followed by the outer flat areas and radius areas.

Finally, the functional parameters relevant to tribological performance (Vmp and Vvv) are shown in Fig. 8. The trends observed corresponded to those described by the height (Sa and Sq) parameters. The inner flat areas presented the biggest values; these were followed by the outer flat areas and the radius areas.

In summary, the mass surface roughness study demonstrated that the three effective areas presented different levels of roughness based on different polishing degrees, different milling strategies, or a combination of both. The roughest areas were the inner flat areas, followed by the outer flat areas. Finally, the radius zones presented the smoothest surfaces. The ranking trend was followed by the height (Sa, Sq), hybrid (Sdq, Sdr) and functional (Vmp, Vvv) parameters. This indicated that the roughest areas presented the biggest average surface slope (Sdq). They presented peaks that were more prone to plastic deformation, more complex surfaces (Sdr) composed by more developed area, more material volume in the peak area (Vmp) that was likely to worn away, and more void volume (Vvv) that was able to retain lubricant and trap debris. All the areas presented similar extreme Sz values, indicating that the extreme values are dominated by defects rather than the polishing degree, with negative skewness value (Ssk) indicating a preference for valleys. Around 65% of the measurements corresponded to anisotropic oriented textures; the majority were oriented perpendicular to the material flow.

3. Numerical analysis

The impact of the local roughness on the drawability of automotive components was evaluated through numerical analysis. AutoForm R8 forming software was used as a forming simulation code.

3.1. Automotive components and materials

Not every industrial component was highly impacted by the tribological behaviour. Overall, components with high draw-in values and low mechanical properties were more susceptible to material flow
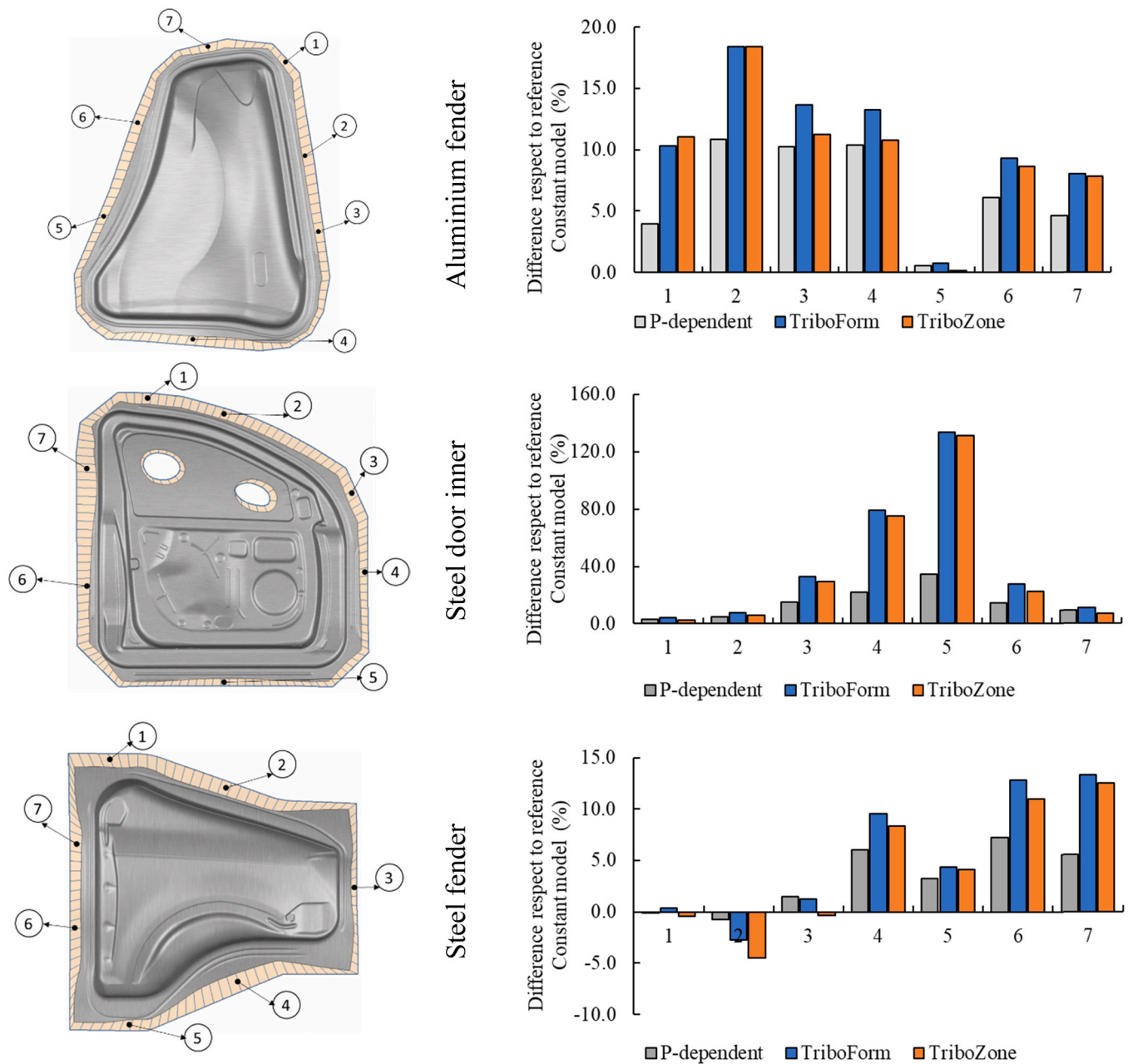
Fig. 11. Draw-in prediction for the three components. On the left side, the draw-in field view under the industry reference case (constant friction model) is shown. Seven points are highlighted per component. On the right side, the difference in draw-in (calculated as a relative percentage to the reference model) is shown for the P-dependent, TriboForm and TriboZone friction models for the seven points under study.

restraining. This restraining (friction) was the result of the specific tribological system, which was defined by the sheet material/roughness, the tool material/roughness, and the lubricant. Therefore, to showcase the potential impact, three high draw-in value components were selected for the study (with approximate draw-in values between 30 mm and 80 mm). These consisted of two fenders (aluminium and steel) and one inner door (steel). Fig. 9 shows the geometry of the three benchmark cases.

The smooth transitions and stretched curvatures that are characteristic of aluminium panels (Fig. 9a) can be observed in comparison to the steel panel (Fig. 9c). As shown in Fig. 9, all benchmark tool designs present draw-beads. Accordingly, the material flow is restrained by both by the draw-bead and the friction on the blank-holding area. This controls the drawing operation and the robustness.

Table 2 summarises the elasto-plastic material behaviour assumed in each component. A hardening model governed by the Swift/Hockett-Sherby expression was assumed for all materials. The Barlat-89 yielding criterion was assumed for the aluminium alloy and the Hill and BBC for the steels.

The binder control was defined as a gap control with zero gap. This means that the binder (also known as the blank-holder) applied the necessary pressure to ensure that the distance between the blank-holder surface and the die surface was equal to the initial sheet thickness. The industrial standard final validation simulation parameters were assumed for each simulation with elasto-plastic shell elements with 11 integration point through thickness.

3.2. Tribology models and simulation procedure

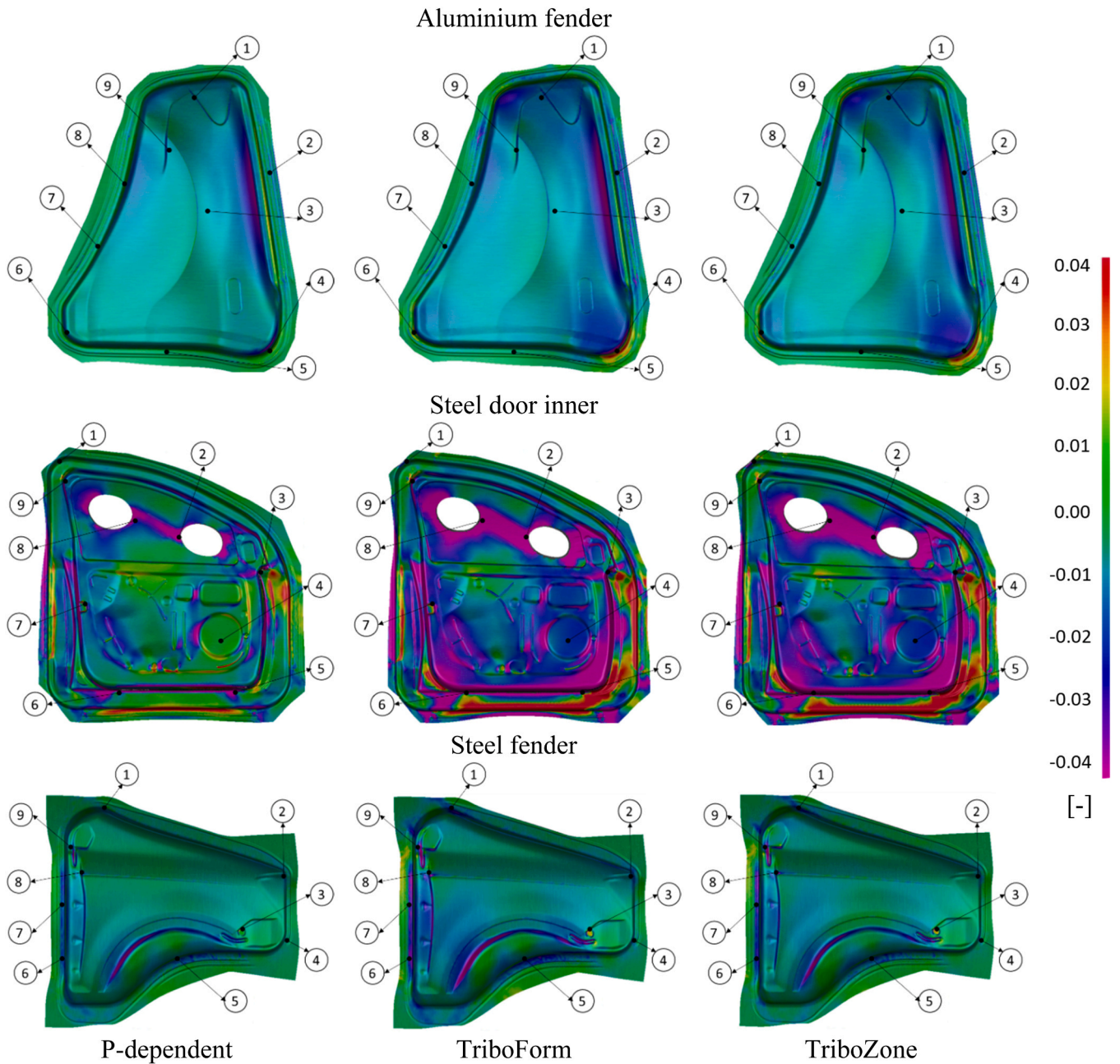In order to analyse the impact of the local roughness, four different

Fig. 12. Field representation of the major strain difference prediction of the advanced models in relation to the industrial reference model (constant friction).

friction models were tested:

1. Constant. The traditional Coulomb constant friction coefficient is the standard in most industrial simulations [30]. Traditionally, a coefficient of 0.15 is taken for steels and a coefficient of 0.12 is taken for aluminium [31]. These were the values assumed in this study in order to be consistent with the industrial experience.
2. P-dependent. The first improvement to the Amonton-Coulomb constant model was to take into account the flattening of the asperities (usually of the sheet material) in an empirical way. This assumed a friction coefficient that decreased when the contact pressure was increased. The use of this type of model has increased in recent years [32]. The evolution of the coefficient was assumed to follow a potential distribution of Filzek:

$$\mu = \mu_b \left(\frac{p}{p_{ref}} \right)^{e-1}, \tag{1}$$

where μ represents the effective friction coefficient, μ_b represents the base coefficient, p and p_{ref} are the local pressure value and the reference pressure, respectively, and e is the pressure exponent [33]. In this study, in order to construct the pressure dependency, industry standard evolutions were assumed for both steel and aluminium components. A reference pressure of 4 MPa (characteristic of the blank-holding area), a pressure exponent of 0.9 and a standard value of base coefficient of 0.15 and 0.12 (for steel and aluminium, respectively) were assumed for the three benchmarks.

3. TriboForm. This complex tribological model included the temperature, material strain and sliding velocity dependency of the friction coefficient. It was implemented through the commercial software
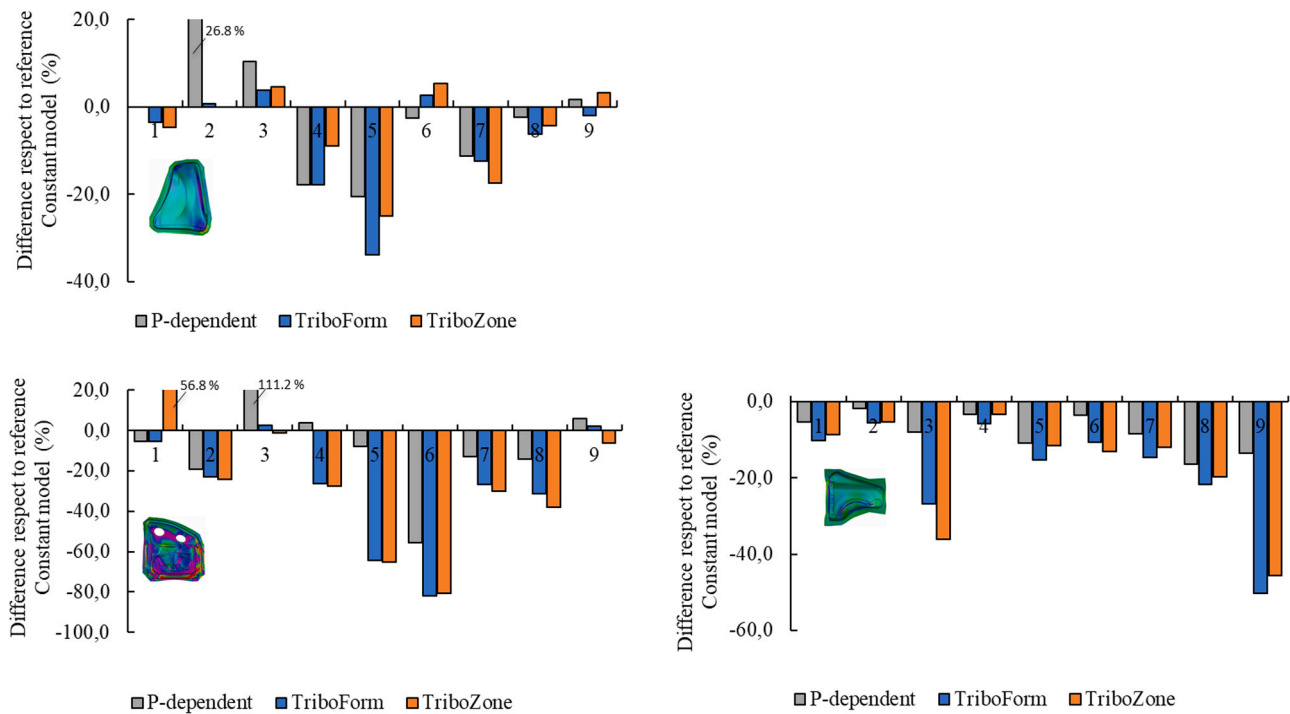
Fig. 13. Major strain difference between the advanced friction models and the industrial reference (constant friction) model for the highlighted nine points. The vertical axis has been limited to 20% for clarity.

TriboForm®. For the aluminium fender component, a tribological pair composed of a sheet material with a roughness of Sa = 1 μm, a cast iron tooling with an average roughness of Sa = 0.98 μm, and a hot melt lubricant layer of 1 g/m2 was assumed. For the steel components, a sheet roughness of Sa = 1.5 μm, a cast iron tool with an averaged roughness of Sa = 0.98 μm, and a lubricant layer of 1 g/m^2 of drawing oil was assumed.

4. TriboZone. In order to evaluate the impact of the tool local roughness, the tool surface was divided into three different effective areas (outer flat areas, inner flat areas, and radius areas; see Fig. 1). Each effective area assumed a TriboForm model considering the different representative local tool surface roughness values characterised in Section 2:
   a. Outer flat area with Sa = 0.98 μm
   b. Inner flat area with Sa = 1.53 μm
   c. Radius area with Sa = 0.71 μm

In this way, each effective area showed a different tribological behaviour due to the different local roughness.

In summary, four different friction models were studied (see Table 3). The ranking considering the increase on complexity and accuracy to resemble the real tribological behaviour is as follows: constant, P-dependent, TriboForm, and TriboZone.

Fig. 10 shows the friction coefficient dependency according to contact pressure for the different friction models. Both aluminium (Fig. 10a) and steel (Fig. 10b) are shown (simulations made considering room temperature, sliding velocity of 50 mm/s, and strain $\bar{\varepsilon}^p = 0$).

Taking the constant model (the industrial standard) as a reference for the aluminium component (Fig. 10a), the P-dependent model presented a trend change at approximately 4 MPa. Under this value, (< 4 MPa), the P-dependent model assumed slightly higher material flow retention (as the friction coefficient is 6% higher on average). The trend was reversed for higher pressures. Assuming that the blank-holding area is usually subjected to pressures between 3 and 5 MPa, a low impact was expected on the material flow between these two friction models. The difference was bigger for higher contact pressures (>20–25 MPa) with

an average coefficient reduction of 15% for the P-dependent case, that will impact on the radius areas (where higher pressures take place). Due to the key role of the draw-beads on the material flow restraining (radius area), an increase on the material flow was expected for the P-dependent friction model (based on industry standard evolution assumptions).

It should be highlighted that the TriboForm friction model presented a bigger complexity compared to the P-dependent model because it took into account the sheet material elasto-plasticity, tool surface roughness, and lubricant. This led to a higher level of prediction accuracy. With the current tribological pair (and under the specific conditions of strain, temperature, and velocity mentioned above), a clear trend change was shown at around 14 MPa. Below this pressure, TriboForm predicted a significantly higher friction coefficient compared to the P-dependent and constant models. As an example, TriboForm predicted a 75% greater coefficient at 5 MPa (0.21) compared to the P-dependent and constant models (0.12). The differences then shifted direction for higher pressures (>15 MPa); the TriboForm model predicted lower friction coefficients. At 35 MPa, TriboForm predicted 61% less friction compared to the constant model (0.047 versus 0.12) and 51% less friction compared to the P-dependent model (0.047 versus 0.096). As mentioned previously, the material flow was driven by the tool design and the influence of both the blank-holder pressure and the draw-bead restriction. As the drawbeads usually present a bigger impact on the material flow control, an increased material flow was expected for the TriboForm model (since lower friction takes place on the high pressure radius areas, e.g the drawbeads) [34].

Regarding the TriboZone friction model (which considers the local tool roughness; Inner flat area Sa= 1.53 μm, outer flat area Sa = 0.98, radius area Sa = 0.71 μm), the main impact took place at low contact pressures (<14 MPa); greater roughness (inner flat area) led to higher friction coefficient distribution. At 5 MPa, for example, the radius and outer flat areas presented coefficients of 0.18 and 0.21, respectively, while the inner flat area showed a coefficient of 0.3. Conversely, negligible differences were observed between the radius and outer flat areas at higher pressures (>14 MPa); the inner flat area presented bigger differences in the range of 18–25 MPa and then converged with the two

Aluminium fender

Steel door inner

Steel fender

P-dependent   TriboForm   TriboZone
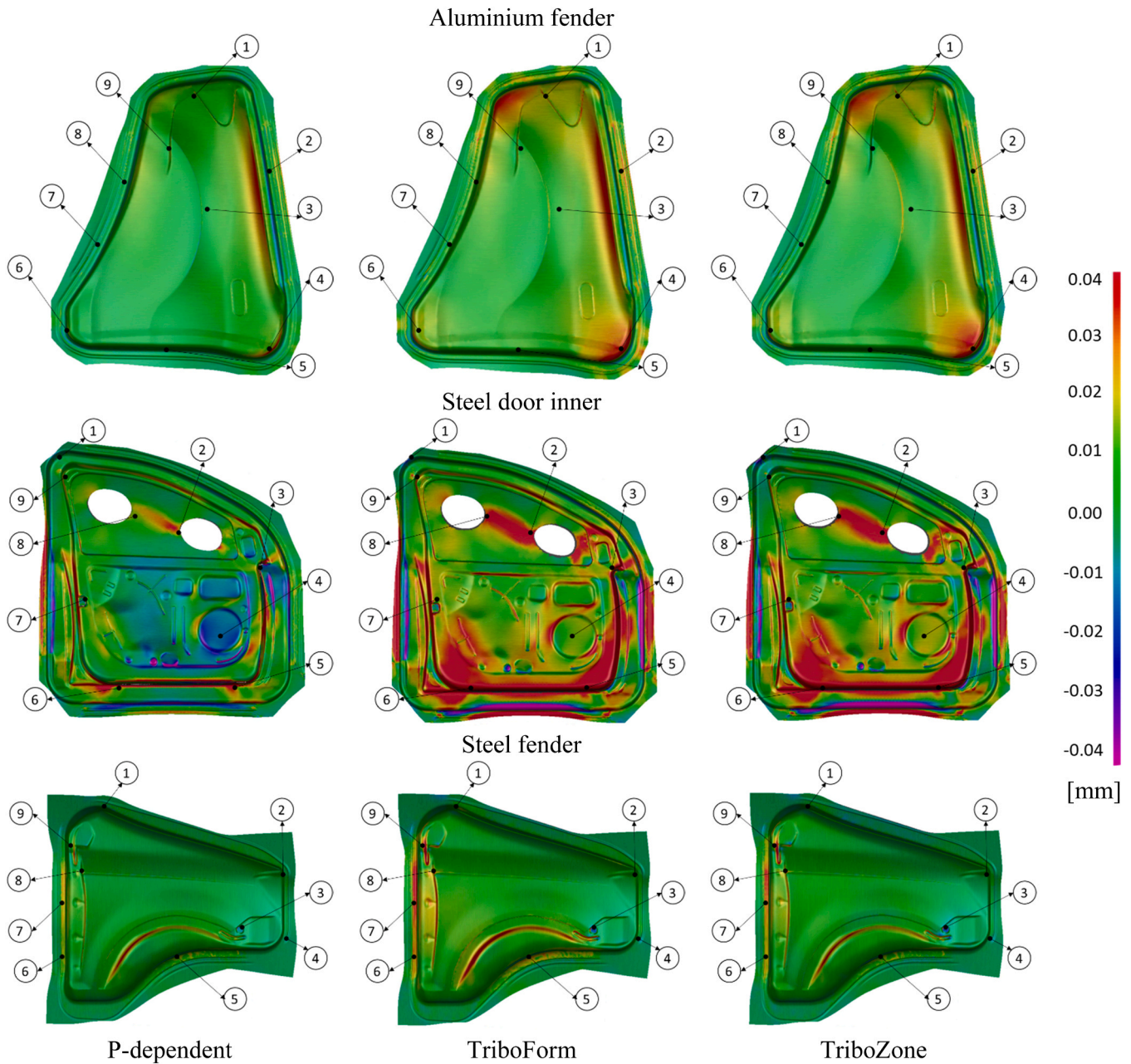
Fig. 14. Field representation of the thinning difference prediction of the advanced models in relation to the industrial reference (constant friction) model. Positive values relate to thinning decrease (less stretching) respect to the reference, and vice versa.

other trends. Taking all these into account, a similar material flow was expected from TriboZone when compared with TriboForm (with a slight smaller material flow expected due to the higher restriction).

In the case of the steel sheet material (Fig. 10b), the differences between the models followed the same trend identified for the aluminium; however, these differences were magnified. The differences between the P-dependent and constant model were similar to those observed for aluminium (Fig. 10a). However, the trend changed with the introduction of the TriboForm friction model at around 18 MPa (instead of at 14 MPa for the aluminium). The TriboZone friction model (considering local roughness) showed similar trend compared to aluminium. However, the inner flat area (high roughness) shows a drastic friction reduction at high pressures (> 20 MPa) in the steel case. Considering that those high pressures are not likely to take place at the inner flat areas, this drastic reduction is likely to have a low impact.

3.3. Drawing results and discussion

All three components were simulated under the four friction models (constant, P-dependent, TriboForm, and TriboZone). The results of all simulations were then compared against the industrial reference (constant). As the friction directly influenced the restraining of the material flow (and therefore the draw-in), the comparisons were performed in terms of draw-in distances, thinning, major strain, and the forming limit diagram (FLD [19]). All simulations were compared on the bottom end of the closing (complete closure of the die). The constant friction model was treated as the industrial reference; the other three models (P-dependent, TriboForm, and TriboZone) were treated as the advanced models due to their increase in features (Table 3).

3.3.1. Draw-in of the material

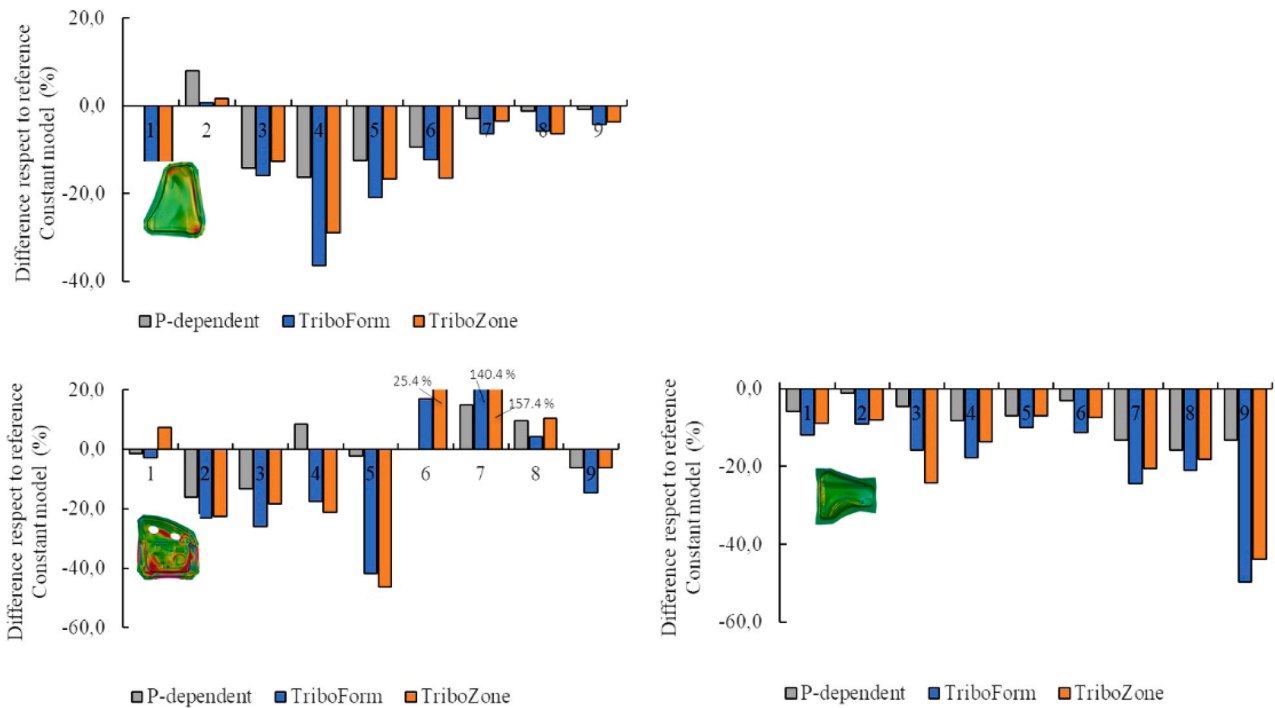The draw-in represents how much the blank edge displace during the

Fig. 15. Thinning difference between the advanced friction models and the industrial reference (constant friction) model for the nine highlighted points.

forming towards the die cavity. Lower draw-in values led to higher strains (and vice versa). Fig. 11 shows the draw-in for the three benchmark cases. On the left side, the draw-in field view of the three components (corresponding to the constant friction model) is shown. Seven representative points are highlighted. On the right side of Fig. 11, the draw-in difference at the seven representative points (calculated as a relative change in respect to the reference) is presented for all the friction models.

Overall Fig. 11 shows that the three friction models under analysis predicted increased draw-in values compared to the reference model (albeit to different extents). The most complex models, (TriboForm and TriboZone) predicted a significantly higher draw-in compared to the P-dependent model. In 80% of the analysed points, the higher draw-in values were predicted by the TriboForm friction model, closely followed by the TriboZone model. As a reference, the draw-in values were around 30–40 mm for the aluminium fender, 30–90 mm of the steel door inner, and 25–60 mm for the steel fender.

The increase in the draw-in denoted a lower restriction of the sheet during forming. The obtained results were in agreement with the previous analysis regarding the friction coefficient dependency on the pressure (Fig. 10), in which similar trends were observed between TriboZone and TriboForm friction models (with slightly less restriction for the latter).

Fig. 12 shows the field representation of the major strain prediction differences for the advanced friction models (P-dependent, TriboForm and TriboZone) in respect to the industrial reference model (constant). Both fender components have a large area in green (representing a difference of zero in the major strain). However, localised areas with a decrease in major strain compared to the constant model were observed (blue and purple zones). These can be associated with a reduction of the stretching derived from the increase of material flow (draw-in). Conversely, the aluminium fender also showed localised major strain increase zones (red areas) for the advanced TriboZone and TriboForm friction models. There was a clear material accumulation in this area (characteristic of the local geometry) that was increased when the draw-in was increased.

The door inner component presented more significant major strain

differences for the three friction models. A relaxation (reduction on major strain) of the area between the window pre-cut holes was observed, with an increase in the material accumulation (increase in major strain) in bottom side. The differences were more significant for the TriboForm and TriboZone friction models, which show a clear resemblance to one another. Overall, the TriboForm model presents the biggest major strain differences, closely followed by the TriboZone model. The P-dependent model was closest to the reference (Constant) model.

Fig. 13 shows the major strain differences of the nine representative points (highlighted in Fig. 12). These are represented as percentage chance with respect to the reference model.

It can be observed that only 48% of the studied 27 points followed the previously observed trend (Fig. 12). Accordingly, it can be concluded that the particularisation of the general rule to specific points of the component might lead to erroneous conclusions.

Fig. 14 shows the field representation of the thinning prediction differences (related to the stretching of the material) of the advanced friction models (P-dependent, TriboForm and TriboZone) in relation to the industrial reference (constant) model.

A negative thinning value was obtained when stretching the material; this was measured in millimetres. Accordingly, the negative values shown in Fig. 14 (thinning differences) relate to thinning increase (more stretching) in relation to the reference model. Positive values relate to thinning decrease (less stretching).

The thinning results directly followed the major strain prediction trends. The thinning or thickening was related to the reaction of the sheet to the stretching or compression of the material on the plane, in order to maintain the volume [35]. Taking into account that the initial material thicknesses were between 0.7 and 1.15 mm, the difference of 0.04 mm (the limit of the legend) represents differences in thickness between 3.4% and 5%. The impact of the friction model on the final thickness was more localised in the fenders (when compared to the door component). However, it should be considered that these differences could be critical at a local level for fulfilling the requirements of the component.

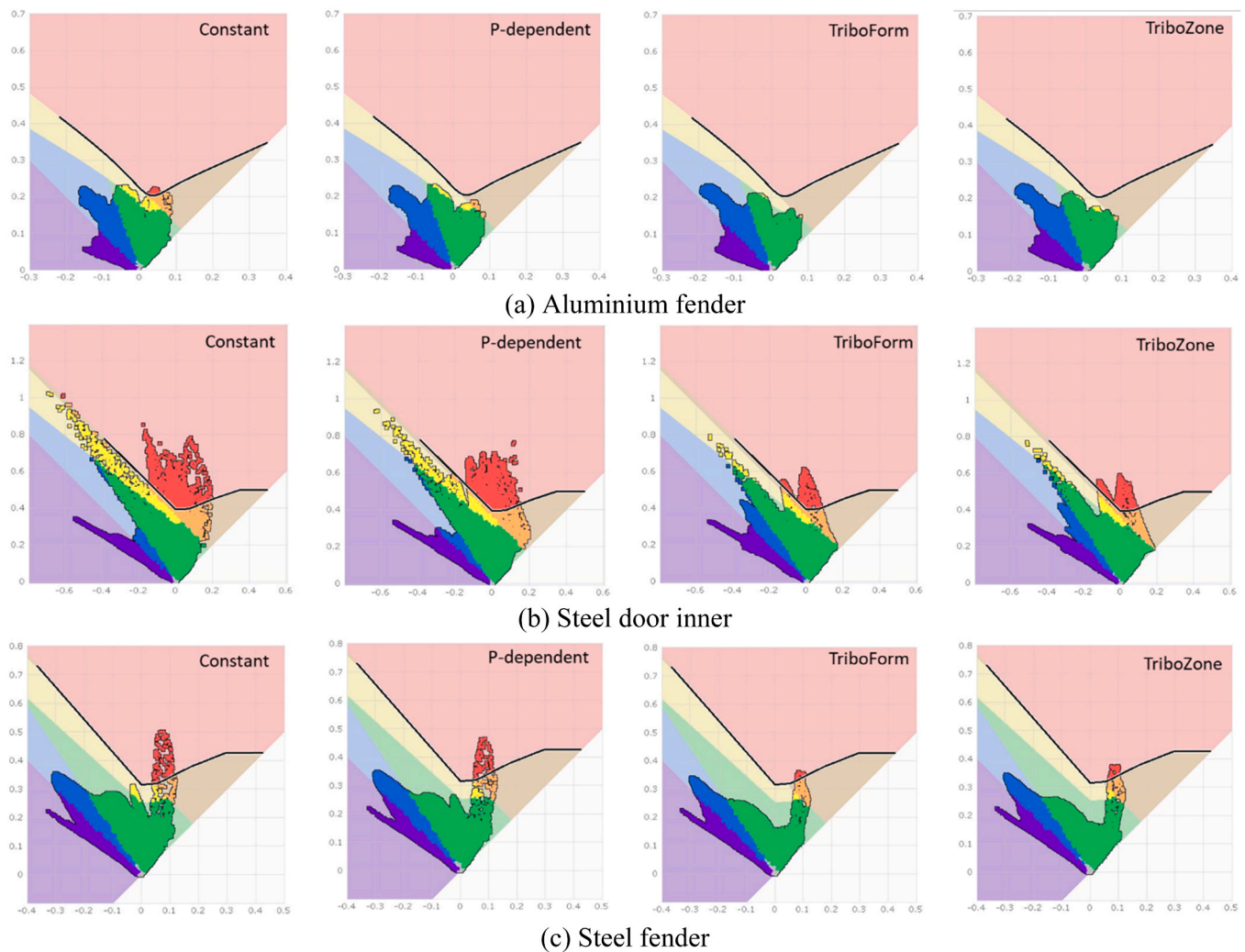Fig. 15 shows the point-to-point representation of the differences in

(a) Aluminium fender

(b) Steel door inner

(c) Steel fender

Fig. 16. FLD diagrams of the benchmark parts in which the FLC and the strain points in the major strain (y axes) and minor strain (x axes) are represented: a) aluminium fender, b) steel inner door, and c) steel fender.

the thinning of the nine points highlighted in Fig. 14.

In this case, 62% of the points followed the global trend. In terms of major strain and thinning, the trends shown (Fig. 12 and Fig. 14) were in accordance with the draw-in results. When the draw-in was increased, the major strain was reduced along with the thinning of the material. However, it was observed that the evolution of local points (Fig. 13 and Fig. 15) did not always follow the general trends due to the complexity of the industrial geometries.

Process engineers use forming limit diagrams (FLDs) as a reference to evaluate the formability of a specific process [36]. This graphical representation shows whether a necking situation will be expected on the try-out step. Fig. 16 shows the FLD diagrams of the benchmarks under the four friction models. The vertical and horizontal axes correspond to the major and minor strains, respectively. The solid curve in the FLD is called the forming limit curve (FLC) and separates the safe and failure zones (a strain state above the FLC implies local necking or fracture). The cloud of points represented on the FLD shows the strain state of each element of the numerical simulation. The points in purple on the left correspond to areas of material that were mainly under compression stresses on the plane. Essentially, the predominant strain is under compression. Accordingly, these points show a higher absolute value of the minor strain compared to the absolute value of the major strain. These points, if situated in the blank-holder/die sandwich area, will tend to increase in thickness but, if out of that area could be a risky area of wrinkles on the part [37].

Fig. 16 shows the FLD diagrams of the benchmarks under the four friction models.

From these FLD representations (see Fig. 16), the impact of the friction model on the drawing prediction output can be clearly observed. As the friction model complexity increases from left to right, a clear reduction in the global stretch state of the component can be observed. When compared to the reference constant model, a significant reduction can be observed for the P-dependent friction model. For the aluminium fender benchmark case, the reference (constant friction) model predicts a non-valid process with necking points (the red area above the FLC). The process is valid for the rest of the friction model cases (all points below FLC). It should be noted, however, that there are the significant differences between the reference (constant) and the TriboForm and TriboZone friction models, at which the strain peaks on the FLD drastically decrease. A clear example of this is found in the case of the steel fender (Fig. 16. (c)), in which the constant and P-dependent friction models predict a broken part (big part above FLC, in red) while assuming TriboForm or TriboZone friction models only a reduced area is slightly above the FLC.

From these FLD representations (in which the overall overview of the component strain field is represented), it can be concluded that in all three benchmark cases the constant friction model leads to the most conservative scenario. A slight reduction on the strain field is appreciated when assuming the P-dependent friction model, and a massive reduction is shown when assuming TriboForm or TriboZone friction

models. These last two models lead to very similar strain distribution; TriboForm leads to lower strain values. Accordingly, it can be concluded that the consideration of the local roughness distribution of the die in the friction model leads to a slight difference in the sheet metal forming numerical predictions.

4. Conclusions

In this study, the impact of the local roughness on a stamping process was analysed. The following conclusions can be draw.

Surface topography mass study:

- A mass study analysing surface topography in different effective areas was conducted.
- The three effective areas presented different roughness values due to different polishing degrees, milling strategies, or a combination of both.
- The radius areas presented the lowest average roughness values, followed by the outer flat areas. The inner flat areas were the roughest.
- Most of the areas presented oriented textures (perpendicular to material flow).
- Height (Sa, Sq, Sz, Ssk), hybrid (Sdq, Sdr), and functional (Vmp, Vvv) topographical parameters were suggested for full description of die surfaces.

Stamping impact of the local roughness:

- Due to the industrial component's complexity, local point tendency can differ from global tendency.
- A direct relationship between the friction coefficient, restraining force, major strain, thinning, and FLD was observed. The lower the friction coefficient, the higher the draw-in of the material (and therefore the smaller the degree of major strain and thinning). This led to lower points on the FLD.
- The observed general trend showed that the constant friction model was the most conservative because it predicted the higher restriction.
- A reduction of the restriction was observed when assuming the P-dependent model. However, greater differences occurred when assuming TriboForm or TriboZone models.
- Both TriboForm and TriboZone models predicted similar results; the TriboForm model predicted less restriction.
- TriboZone model (which considers the local roughness) did not lead to critical differences when compared to TriboForm assumptions.

In view of these results and the cost efficiency of implementing all four models, the authors recommend the use of the TriboForm friction model for feasibility studies. Local roughness has been shown to have a moderate impact; this data may be of interest at mature process optimisation stages. Further investigations are needed to investigate the impact of the present findings with industrial experimental data.

CRediT authorship contribution statement

Alaitz Zabala: Conceptualization, Methodology, Validation, formal analysis, Resources, Writing – Original Draft, Supervision. **Eneko Sáenz de Argandoña**: Conceptualization, Methodology, formal analysis, Resources, Writing – Review & Editing. **Daniel Cañizares**: Software, Validation. **Iñigo Llavori**: Software, Formal analysis, Writing – Review & Editing, Visualization. **Nagore Otegi**: Software, Formal analysis, Writing – Review & Editing. **Joseba Mendiguren**: Conceptualization, Methodology, Validation, Formal analysis, Resources, Writing – Original Draft, Supervision, Project administration, Funding acquisition.

Declaration of Competing Interest

The authors declare that they have no known competing financial interests or personal relationships that could have appeared to influence the work reported in this paper.

References

[1] Böhm T, Meurer T. Trajectory planning for a deep drawing tool. IFAC Proc Vol 2014;19:665–70. https://doi.org/10.3182/20140824-6-za-1003.01565.

[2] Sigvant M, Pilthammar J, Hol J, Wiebenga JH, Chezan T, Carleer B, et al. Friction in sheet metal forming: influence of surface roughness and strain rate on sheet metal forming simulation results. Procedia Manuf 2019;29:512–9. https://doi.org/10.1016/j.promfg.2019.02.169.

[3] Pilthammar J, Sigvant M, Kao-Walter S. Introduction of elastic die deformations in sheet metal forming simulations. Int J Solids Struct 2018;151:76–90. https://doi.org/10.1016/j.ijsolstr.2017.05.009.

[4] Pereira MP, Yan W, Rolfe BF. Contact pressure evolution and its relation to wear in sheet metal forming. Wear 2008;265:1687–99. https://doi.org/10.1016/j.wear.2008.04.042.

[5] Zabala A, Llavori I, Sáenz de Argandoña E, Mendiguren J. Towards the automation of the die spotting process: contact blue pattern decryption. J Manuf Process 2020; 58:1285–96. https://doi.org/10.1016/j.jmapro.2020.09.022.

[6] Essig P, Liewald M, Bolay C, Schubert T. Digital process support in toolmaking by using optical metrology. IOP Conf Ser Mater Sci Eng 2019:651. https://doi.org/10.1088/1757-899X/651/1/012026.

[7] Tatipala S, Pilthammar J, Sigvant M, Wall J, Johansson CM. Introductory study of sheet metal forming simulations to evaluate process robustness. IOP Conf Ser Mater Sci Eng 2018:418. https://doi.org/10.1088/1757-899X/418/1/012111.

[8] Barlat F, Yoon SY, Lee SY, Wi MS, Kim JH. Distortional plasticity framework with application to advanced high strength steel. Int J Solids Struct 2020;202:947–62. https://doi.org/10.1016/j.ijsolstr.2020.05.014.

[9] Sun L, Wagoner RH. Complex unloading behavior: nature of the deformation and its consistent constitutive representation. Int J Plast 2011;27:1126–44.

[10] Mendiguren J, Cortés F, Galdos L. A generalised fractional derivative model to represent elastoplastic behaviour of metals. Int J Mech Sci 2012;65:12–7.

[11] Pilthammar J, Sigvant M, Hansson M, Pálsson E, Rutgersson W. Characterizing the elastic behaviour of a press table through topology optimization. J Phys Conf Ser 2017:896. https://doi.org/10.1088/1742-6596/896/1/012068.

[12] Szakaly ED, Lenard JG. The effect of process and material parameters on the coefficient of friction in the flat-die test. J Mater Process Technol 2010;210: 868–76. https://doi.org/10.1016/j.jmatprotec.2010.01.019.

[13] Shisode M, Hazrati J, Mishra T, de Rooij M, Horn C, van Beeck J, et al. Modeling boundary friction of coated sheets in sheet metal forming. Tribol Int 2021;153: 106554. https://doi.org/10.1016/j.triboint.2020.106554.

[14] Mishra T, Ganzenmüller GC, de Rooij M, Shisode M, Hazrati J, Schipper DJ. Modelling of ploughing in a single-asperity sliding contact using material point method. Wear 2019;418–419:180–90. https://doi.org/10.1016/j.wear.2018.11.020.

[15] Masters IG, Williams DK, Roy R. Friction behaviour in strip draw test of pre-stretched high strength automotive aluminium alloys. Int J Mach Tools Manuf 2013;73:17–24. https://doi.org/10.1016/j.ijmachtools.2013.05.002.

[16] Shisode M, Hazrati J, Mishra T, De Rooij M, Van Den Boogaard T. Evolution of real area of contact due to combined normal load and sub-surface straining in sheet metal. Friction 2020;9:840–55. https://doi.org/10.1007/s40544-020-0444-6.

[17] Heingärtner J, Veldhuis M, Kott M, Hora P. Process control of forming processes to compensate temperature induced friction changes. Procedia Manuf 2020;47: 547–52. https://doi.org/10.1016/j.promfg.2020.04.164.

[18] Kott M, Erz C, Heingärtner J, Groche P. Controllability of temperature induced friction effects during deep drawing of car body parts with high drawing depths in series production. Procedia Manuf 2020;47:553–60. https://doi.org/10.1016/j.promfg.2020.04.166.

[19] Waanders D, Marangalou JH, Kott M, Gastebois S, Hol J. Temperature dependent friction modelling: the influence of temperature on product quality. Procedia Manuf 2020;47:535–40. https://doi.org/10.1016/j.promfg.2020.04.159.

[20] Veldhuis M, Heingärtner J, Krairi A, Waanders D, Hazrati J. An industrial-scale cold forming process highly sensitive to temperature induced frictional start-up effects to validate a physical based friction model. Procedia Manuf 2020;47: 578–85. https://doi.org/10.1016/j.promfg.2020.04.176.

[21] Hettich D, Aha B, Zimmermann R, Veldhuis M, Filzek J. Lubricant- Reducing scrap rates in forming high-alloyed steel by stable friction behavior over the temperature. Procedia Manuf 2020;47:561–5. https://doi.org/10.1016/j. promfg.2020.04.168.

[22] Hol J, Wiebenga JH, Stock J, Wied J, Wiegand K, Carleer B. Improving stamping simulation accuracy by accounting for realistic friction and lubrication conditions: spplication to the door-outer of the Mercedes-Benz C-class Coupé. J Phys Conf Ser 2016:734. https://doi.org/10.1088/1742-6596/734/3/032091.

[23] Sigvant M, Pilthammar J, Hol J, Wiebenga JH, Chezan T, Carleer B, et al. Friction and lubrication modelling in sheet metal forming simulations of the Volvo XC90 inner door. J Phys Conf Ser 2016:734. https://doi.org/10.1088/1742-6596/734/3/032090.

[24] Hol J, Wiebenga JH, Carleer B. Friction and lubrication modelling in sheet metal forming: Influence of lubrication amount, tool roughness and sheet coating on product quality. J Phys Conf Ser 2017:896. https://doi.org/10.1088/1742-6596/896/1/012026.

[25] Sigvant M, Pilthammar J, Hol J, Wiebenga JH, Chezan T, Carleer B, et al. Friction in sheet metal forming simulations: modelling of new sheet metal coatings and lubricants. IOP Conf Ser Mater Sci Eng 2018:418. https://doi.org/10.1088/1757-899X/418/1/012093.

[26] ISO 25178-2 2012 Geometrical product specifications (GPS)- Surface texture: Areal: II. terms, definitions and surface texture parameters; 2012.

[27] Zabala A, Blunt L, Aginagalde A, Llavori I, Tato W. Development of a novel method to characterize mean surface peak curvature as a signature of tribological performance of dental implant surfaces. Surf Topogr Metrol Prop 2020;8:024001. https://doi.org/10.1088/2051-672X/ab82a3.

[28] Sedlaček M, Podgornik B, Vižintin J. Correlation between standard roughness parameters skewness and kurtosis and tribological behaviour of contact surfaces. Tribol Int 2012;48:102–12. https://doi.org/10.1016/j.triboint.2011.11.008.

[29] Blateyron F. The areal field parameters. Characterisation Areal Surf. Texture. Berlin, Heidelberg: Springer Berlin Heidelberg; 2013. p. 15–43. https://doi.org/10.1007/978-3-642-36458-7_2.

[30] Andersson A. Numerical and experimental evaluation of springback in a front side member. J Mater Process Technol 2005;169:352–6. https://doi.org/10.1016/j.jmatprotec.2005.04.095.

[31] Mendiguren J, Agirre J, Mugarra E, Galdos L, De Argandoña ES. Sensitivity analysis on an AC600 aluminum skin component. J Phys Conf Ser 2016:734. https://doi.org/10.1088/1742-6596/734/3/032035.

[32] Gil I, Mendiguren J, Galdos L, Mugarra E, Saenz de Argandoña E. Influence of the pressure dependent coefficient of friction on deep drawing springback predictions. Tribol Int 2016:103. https://doi.org/10.1016/j.triboint.2016.07.004.

[33] Filzek J, Ludwig M, Groche P. Improved FEM Simulation of Sheet Metal Forming with Friction Modelling using Laboratory Tests. Proc. IDDRG, Bilbao; 2011.

[34] Bolay C, Essig P, Kaminsky C, Hol J, Naegele P, Schmidt R. Friction modelling in sheet metal forming simulations for aluminium body parts at Daimler AG. IOP Conf Ser: Mater Sci Eng 2019;651:012104. https://doi.org/10.1088/1757-899X/651/1/012104.

[35] Banabic D. Sheet metal forming processes: constitutive modelling and numerical simulation. Springer Science & Business Media; 2010.

[36] Yang Z, Zhao C, Dong G, Chen Z. Experimental calibration of ductile fracture parameters and forming limit of AA7075-T6 sheet. J Mater Process Technol 2021;291:117044. https://doi.org/10.1016/j.jmatprotec.2021.117044.

[37] Shinge VR, Dabade UA. Experimental investigation on forming limit diagram of mild carbon steel sheet. Procedia Manuf 2018;20:141–6. https://doi.org/10.1016/j.promfg.2018.02.020.